

A combined proteomic and targeted analysis unravels new toxic mechanisms for zinc oxide nanoparticles in macrophages

Catherine Aude-Garcia, Bastien Dalzon, Jean-Luc Ravanat, Véronique Collin-Faure, Hélène Diemer, Jean-Marc Strub, Sarah Cianférani, Alain van Dorsselaer, Marie Carrière, Alain Van Dorsselaer, et al.

▶ **To cite this version:**

Catherine Aude-Garcia, Bastien Dalzon, Jean-Luc Ravanat, Véronique Collin-Faure, Hélène Diemer, et al.. A combined proteomic and targeted analysis unravels new toxic mechanisms for zinc oxide nanoparticles in macrophages. Journal of Proteomics, 2016, 134, pp.174 - 185. 10.1016/j.jprot.2015.12.013 . hal-01691352

HAL Id: hal-01691352
https://hal.science/hal-01691352

Submitted on 23 Jan 2018

HAL is a multi-disciplinary open access archive for the deposit and dissemination of scientific research documents, whether they are published or not. The documents may come from teaching and research institutions in France or abroad, or from public or private research centers.

L'archive ouverte pluridisciplinaire **HAL**, est destinée au dépôt et à la diffusion de documents scientifiques de niveau recherche, publiés ou non, émanant des établissements d'enseignement et de recherche français ou étrangers, des laboratoires publics ou privés.

This document is an author version of a paper published in Journal of Proteomics (2016) under the doi: 10.1016/j.jprot.2015.12.013

A combined proteomic and targeted analysis unravels new toxic mechanisms for zinc oxide nanoparticles in macrophages

Catherine Aude-Garcia [1,2,3] , Bastien Dalzon [1,2,3], Jean-Luc Ravanat [4,5] , Véronique Collin-Faure [1,2,3] Hélène Diemer [6], Jean Marc Strub [6] , Sarah Cianferani [6], Alain Van Dorsselaer [6], Marie Carrière [4,5] , Thierry Rabilloud [1,2,3]*

1: CEA Grenoble, iRTSV/CBM, Laboratory of Chemistry and Biology of Metals, Grenoble, France

2: Univ. Grenoble Alpes, Laboratory of Chemistry and Biology of Metals, Grenoble, France

3: CNRS UMR 5249, Laboratory of Chemistry and Biology of Metals, Grenoble, France

4: Univ. Grenoble Alpes, INAC, SCIB, F-38000 Grenoble, France.

5: CEA, INAC-SCIB/LAN F-38000 Grenoble, France.

6: Laboratoire de Spectrométrie de Masse BioOrganique (LSMBO), Université de Strasbourg, IPHC, 25 rue Becquerel 67087 Strasbourg, France. CNRS, UMR7178, 67037 Strasbourg, France.

*: to whom correspondence should be addressed:
Laboratoire de Chimie et Biologie des Métaux, UMR CNRS-CEA-UJF 5249, iRTSV/LCBM, CEA Grenoble, 17 rue des martyrs, F-38054 Grenoble Cedex 9, France
thierry.rabilloud@cea.fr

Abstract

The cellular responses of the J774 macrophage cell line to zinc oxide and zirconium oxide nanoparticles have been studied by a comparative quantitative, protein level based proteomic approach. The most prominent results have been validated by targeted approaches. These approaches have been carried out under culture conditions that stimulate mildly the aryl hydrocarbon receptor, thereby mimicking conditions that can be encountered in vivo in complex environments. The comparative approach with two nanoparticles allows to separate the common responses, which can be attributed to the phagocytosis event per se, from the response specific to each type of nanoparticles.
The zinc-specific responses are the most prominent ones and include mitochondrial proteins too, but also signaling molecules such as MyD88, proteins associated with methylglyoxal detoxification (glyoxalase 2, aldose reductase) and deoxyribonucleotide hydrolases. The in cellulo inhibition of GAPDH by zinc was also documented, representing a possible source of methylglyoxal in the cells, leading to an increase in methylglyoxal-modified DNA bases. These observations may be mechanistically

associated with the genotoxic effect of zinc and its selective effects on cancer cells.

KEYWORDS
Nanoparticles; macrophages; zinc oxide; zirconium dioxide; proteomics; glutathione biosynthesis; phagocytosis; DNA damage; heme oxygenase; methyglyoxal; mitochondria

1. Introduction

Metal oxide nanoparticles are more and more used in the industry for various purposes, which poses the problem of assessing the hazard they can cause to humans and to the environment. This poses in turn the problem of assessing the danger represented by the metal oxide nanoparticles, and this danger appears to vary widely with the chemical nature of the metal oxide [1]. In this context, zinc oxide appears among the toxic nanoparticles, although it has obvious industrial interests, e.g. as a biocide [2], or used in tyres and in sunscreens [3]. The toxicity of zinc oxide is indeed known for decades, as it is one causative agent of metal fume fever [4] [5].
There has been quite active research to determine the toxic mechanisms of these nanoparticles, and many papers imply the oxidative stress pathway, [6, 7], leading to DNA damage and genotoxicity in vitro [8-11] but also in vivo [12, 13], although this is still a controversial issue [14].
Among the several cell types that are relevant to be studied for the in vitro assessment of the toxicity of nanoparticles and of their toxic mechanism, macrophages represent an important cell type, because of their critical role in immunity and in inflammation, and the inflammation parameters have been investigated for several nanomaterials (e.g. in [15]).
In this respect, macrophages are also very sensitive to their environment, for example via the aryl hydrocarbon receptor (AHR). This receptor has a wide variety of ligands, either from anthropogenic sources such as dioxins [16] or natural ones such as tryptophan derivatives [17-20]. Binding of these ligands to the AHR receptor induces important protein expression changes in several cell types [21] and has profound effects on immune cells [22]. Because of the variety of situations leading to stimulation of the AHR, many of which being likely to occur in complex environments such as natural and urban ones, it is of interest to investigate the response of macrophages to nanoparticles under conditions where the AHR is mildly stimulated. Such conditions can be reached quite simply by changing the culture medium of the cells. Because of its high content in aromatic amino acids, DMEM stimulates the AHR [20], leading to the well-described immunosuppressive effects associated to AHR stimulation in macrophages [19, 23].

Proteomics studies are rather uncommon in the field of nanotoxicology [24], although recent studies have investigated the effects of silver nanoparticles on colon cell lines [25] or of copper oxide on lung epithelial cells [26]. Despite their relatively scarce use, all proteomic studies have shown a potential to unravel interesting cellular responses, e.g. mitochondrial responses [25, 27], cytoskeletal responses [26], or metabolic ones [28], metabolic responses being also demonstrated by targeted studies [29]. This is why, in addition to our previous work [28, 30] carried out in RPMI, a medium that does not stimulate the AHR [20], we have undertaken a proteomic study of the responses of macrophages to zinc oxide nanoparticles in AHR-stimulating conditions, i.e. in DMEM-cultured cells, zirconium oxide being used as a negative, non toxic control [27].

2. Material and methods

2.1. Nanoparticles

Zinc oxide (catalog number# 721077) and zirconium oxide (catalog number# 643025) were purchased from Sigma (Saint Quentin Fallavier, France). Zirconium oxide was coated with PVP 40 (purchased from Sigma) as previously described [27]. Zinc oxide was used as provided by the manufacturer. The characterization of the nanoparticles has been described previously [27, 28, 30]. The hydrodynamic diameter and the particle size distribution were characterized by dynamic light scattering (DLS) after dilution in complete culture medium using a Wyatt Dynapro Nanostar instrument. We also verified previously that PVP alone had no effects on the cells [30].

2.2. Cell culture

The mouse macrophage cell line J774A1 was purchased from the European Cell Culture Collection (Salisbury, UK). The cells were cultured in DMEM (containing 1mM pyruvate) + 10% fetal bovine serum. Cells were seeded every two days at 200,000 cells/ml and harvested at 1,000,000 cells per ml. For treatment with nanoparticles, the following scheme was used: cells were first seeded at 500,000 cells/ml in T175 flasks (50 ml per flask). They were exposed to zinc oxide nanoparticles (or to the equivalent concentration of zinc acetate) on the following day and harvested after a further 24 hours in culture. Cell viability was measured by trypan blue exclusion.
Under these culture conditions, the LD20 was determined to be 8µg/ml for zinc oxide, 600µM for methylglyoxal, and could not be reached for zirconium oxide even at 100µg/ml. Thus, zinc oxide was used at its LD20 concentrations, while zirconium oxide was used at 10µg/ml to provide a control for phagocytosis of a non toxic particle in the same size range and density (and thus particle number) as the more toxic zinc oxide nanoparticles.

2.3. F-Actin staining

J774 cells were cultured on coverslips placed in 6-well plates and exposed to NPs for 24h at 37°C. At the end of the exposure time, cells were washed twice for 5 min at 4°C in PBS, fixed in 4% paraformaldehyde for 30 min at room temperature. After two washes (5min/4°C in PBS), they were permeabilized in Triton X100 0.1% for 5 min at room temperature. After two more washes in PBS, 500 nM Phalloidin-Atto 550 (Sigma) was added to the cells and let for 20 min at room temperature in the dark. Coverslips-attached cells were washed, placed on microscope slides (Thermo Scientific) using a Vectashield mounting medium containing DAPI (Eurobio) and imaged using a Leica TCS SP2 SE confocal microscope. The images were processed using the Leica confocal software.

2.4. Phagocytosis activity measurement

The phagocytic activity was measured after treatment with either zinc oxide and zirconium oxide nanoparticles using fluorescent latex beads (1µm diameter, green labelled, catalog number L4655 from Sigma) and flow cytometry, essentially as described in [27, 31].

2.5. Mitochondrial transmembrane potential measurement.

After exposure to the nanoparticles for 24 hours, the mitochondrial transmembrane

potential of the cells was assessed by JC-carbocyanine probes fluorescence [32], using the water soluble JC-10 probe[33] . Briefly, cells were treated with 10 µM JC-10 in complete culture medium for 30 minutes at 37 °C. Cells were then harvested, rinsed twice in PBS + 1mg/ml glucose and analysed by flow cytometry on a FACScalibur instrument (Beckton Dickinson). First the live cells were selected on the basis of the size and granularity, then the fluorescence of these live cells was measured using excitation at 488 nm and emission of the J-aggregates at 590 nm.

2.6. GAPDH assay

The cell extracts for enzyme assays were prepared by lysing the cells for 20 minutes at 0°C in Hepes 20 mM pH 7.5, MgCl2 2 mM, KCl 50 mM, EGTA 1 mM, SB 3-14 0.15% w/v, followed by centrifugation at 15,000g for 15 minutes to clear the extract. The protein concentration was determined by a dye-binding assay [34]. The GAPDH activity was assayed by a coupled assay using Nitro blue tetrazolium as the final acceptor and phenazine methosulfate as a relay [35]
For the zinc inhibition studies, the cell extracts were first diluted in the assay buffer (final protein concentration 0.2 mg/ml), and supplemented with defined concentrations of zinc acetate. The resulting solutions were incubated at 37°C for 30 minutes to allow zinc binding. The substrates and cofactors were then added and the activity measured spectrophotometrically [35].

2.7. Detection of dG-MG adducts :

Quantitative measurement of methylglyoxal dGuo adducts (dG-MG) were performed by isotope dilution high performance liquid chromatography coupled to tandem mass spectrometry (HPLC-MS/MS) [36] subsequently to DNA extraction and digestion performed as previously described [37]. The methyl glyoxal dG adducts and the corresponding isotopically labeled internal standards were prepared by reacting methylglyoxal with dG and $^{15}N_5$-dG, respectively [38]. Detection of the dG-MG adducts was performed in the so-called mrm mode using an Accela HPLC system interfaced with a Quantum Ultra mass spectrometry, as described elsewhere [38] with minor modifications. Separation was performed using an Uptishere ODB 3µm octadecyl silica gel column 150 x 2 mm, 3 µm obtained from Interchim (Montluçon, France) using a linear gradient of methanol from 0 to 30% in 30 min in 2 mM ammonium formate, the flow rate being 0.2 ml/min. Under these conditions, the two isomers of dG-MG (as well as the isotopically labeled internal standards) are eluted at 24.3 and 25.9 min, whereas, dG is eluted at 14.2 min. Transitions 340 →224 and 345→229 (positive ionization mode) were used to detected dG-MG and the M+5 isotopically labeled internal standard (collision energy 33 v), respectively. In addition, transition 270→154 (collision energy 15) was used to detect unmodified 2'-deoxyguanosine (dG) and thus results are expressed as the number of dG-MG adducts per million normal nucleosides.

2.8. Proteomics

The 2D gel based proteomic experiments were essentially carried out as previously described [27]. However, detailed material and methods are provided.

2.8.1. General strategy

All experiments were carried out at least on independent biological triplicates. As the experimental setup involves a comparison of several treatments with the same control group, an additional independent set of samples from untreated cells was also compared to the same control reference group, thereby realizing a true null experiment between the test control group and the reference control group. All the proteins showing the same type of variation (increase or decrease, $p<0.05$) in all groups (including the test control group) compared to the reference control group were discarded from the results.

2.8.2. Sample preparation

The cells were collected by scraping, and then washed three times in PBS. The cells were then washed once in TSE buffer (Tris-HCl 10 mM pH 7.5, sucrose 0.25M, EDTA 1 mM), and the volume of the cell pellet was estimated. The pellet was resuspended in its own volume of TSE buffer. Then 4 volumes (respective to the cell suspension just prepared) of concentrated lysis buffer (urea 8.75 M, thiourea 2.5 M, CHAPS 5% w/v, TCEP-HCl, 6.25 mM, spermine base 12.5 mM) were added and the solution was let to extract at room temperature for 1 hour. The nucleic acids were then pelleted by ultracentrifugation (270,000 g at room temperature for 1 h), and the protein concentration in the supernatant was determined by a dye-binding assay [34]. Carrier ampholytes (Pharmalytes pH 3-10) were added to a final concentration of 0.4% (w/v), and the samples were kept frozen at -20°C until use.

2.8.3. Isoelectric focusing

Home-made 160 mm long 4-8 linear pH gradient gels [39] were cast according to published procedures [40]. Four mm-wide strips were cut, and rehydrated overnight with the sample, diluted in a final volume of 0.6 ml of rehydration solution (7 M urea, 2 M thiourea, 4% CHAPS, 0.4% carrier ampholytes (Pharmalytes 3-10) and 100mM dithiodiethanol [41, 42].
The strips were then placed in a Multiphor plate (GE Healthcare), and IEF was carried out with the following electrical parameters: 100V for 1 hour, then 300V for 3 hours, then 1000V for 1 hour, then 3400 V up to 60-70 kVh. After IEF, the gels were equilibrated for 20 minutes in Tris 125mM, HCl 100mM, SDS 2.5%, glycerol 30% and urea 6 M [43] . They were then transferred on top of the SDS gels and sealed in place with 1% agarose dissolved in Tris 125mM, HCl 100mM, SDS 0.4% and 0.005% (w/v) bromophenol blue. By combining the electrendosmotic flow reduction afforded by the urea-glycerol mixture to a better blocking of thiols, it has been shown [42, 44] that this procedure afford better final results than the classical one using iodoacetamide during the equilibration procedure only [43].

2.8.4. SDS electrophoresis and protein detection

Ten percent gels (160x200x1.5 mm) were used for protein separation. The Tris taurine buffer system [45] was used and operated at a ionic strength of 0.1 and a pH of 7.9. The final gel composition is thus Tris 180mM, HCl 100 mM, acrylamide 10% (w/v), bisacrylamide 0.27%. The upper electrode buffer is Tris 50 mM, Taurine 200 mM, SDS 0.1%. The lower electrode buffer is Tris 50 mM, glycine 200 mM, SDS

0.1%. The gels were run at 25V for 1hour, then 12.5W per gel until the dye front has reached the bottom of the gel. Detection was carried out by a tetrathionate silver staining [46] .

2.8.5. Image analysis

The gels were scanned after silver staining on a flatbed scanner (Epson perfection V750), using a 16 bits grayscale image acquisition. The gel images were then analyzed using the Delta 2D software (v 3.6). Spots that were never expressed above 100 ppm of the total spots were first filtered out. Then, significantly-varying spots were selected on the basis of their Student T-test p-value between the treated and the control groups. Spots showing a p-value lower than 0.05 were selected. This strategy is used to avoid the use of arbitrary thresholds, which can result in discarding statistically-valid relevant changes and including non-valid changes [47]. The multiple testing problem was addressed using the Storey-Tishirani approach [48], as classical statistical filters (e.g. Bonferroni or Benjamini-Hochberg) yield to over-rejection of valid results [49]. Furthermore, we checked that all the spots that we found through the T-test had also a $p<0.05$ in a non parametric Mann-Whitney U-test.

2.8.6. Mass spectrometry

The spots selected for identification were excised from silver-stained gels and destained with ferricyanide/thiosulfate on the same day as silver staining in order to improve the efficiency of the identification process [50, 51] . In gel digestion was performed with an automated protein digestion system, MassPrep Station (Waters, Milford, USA). The gel plugs were washed twice with 50 µL of 25 mM ammonium hydrogen carbonate (NH_4HCO_3) and 50 µL of acetonitrile. The cysteine residues were reduced by 50 µL of 10 mM dithiothreitol at 57°C and alkylated by 50 µL of 55 mM iodoacetamide. After dehydration with acetonitrile, the proteins were cleaved in gel with 10 µL of 12.5 ng/µL of modified porcine trypsin (Promega, Madison, WI, USA) in 25 mM NH_4HCO_3. The digestion was performed overnight at room temperature. The generated peptides were extracted with 30 µL of 60% acetonitrile in 0.1% formic acid. Acetonitrile was evaporated under vacuum before nanoLC-MS/MS analysis.
NanoLC-MS/MS analysis was performed using a nanoACQUITY Ultra-Performance-LC (Waters Corporation, Milford, USA) coupled to the Synapt™ High Definition Mass Spectrometer™ (Waters Corporation, Milford, USA). The system was fully controlled by MassLynx 4.1 SCN639 (Waters Corporation, Milford, USA).
The nanoLC system was composed of ACQUITY UPLC® CSH130 C18 column (250 mm x 75 µm with a 1.7 µm particle size, Waters Corporation, Milford, USA) and a Symmetry C18 precolumn (20 mm × 180 µm with a 5 µm particle size, Waters Corporation, Milford, USA). The solvent system consisted of 0.1% formic acid in water (solvent A) and 0.1% formic acid in acetonitrile (solvent B). 4 µL of sample were loaded into the enrichment column during 3 min at 5 µL/min with 99% of solvent A and 1% of solvent B. Elution of the peptides was performed at a flow rate of 300 nL/min with a 8-35% linear gradient of solvent B in 9 minutes.
The tandem mass spectrometer was equipped with a Z-spray ion source and a lock mass system. The capillary voltage was set at 2.8 kV and the cone voltage at 35 V. Mass calibration of the TOF was achieved using fragment ions from Glu-fibrino-peptide B on the [50;2000] m/z range. Online correction of this calibration was

performed with Glu-fibrino-peptide B as the lock-mass. The ion $(M+2H)^{2+}$ at m/z 785.8426 was used to calibrate MS data and the fragment ion $(M+H)^{+}$ at m/z 684.3469 was used to calibrate MS/MS data during the analysis.
For tandem MS experiments, the system was operated with automatic switching between MS (0.5 s/scan on m/z range [150;1700]) and MS/MS modes (0.5 s/scan on m/z range [50;2000]). The two most abundant peptides (intensity threshold 20 counts/s), preferably doubly and triply charged ions, were selected on each MS spectrum for further isolation and CID fragmentation using collision energy profile. Fragmentation was performed using argon as the collision gas.
Mass data collected during analysis were processed and converted into .pkl files using ProteinLynx Global Server 2.3 (Waters Corporation, Milford, USA). Normal background subtraction type was used for both MS and MS/MS with 5% threshold and polynomial correction of order 5. Smoothing was performed on MS/MS spectra (Savitsky-Golay, 2 iterations, window of 3 channels). Deisotoping was applied for MS (medium desisotoping) and for MS/MS (fast deisotoping).
For protein identification, the MS/MS data were interpreted using a local Mascot server with MASCOT 2.4.1 algorithm (Matrix Science, London, UK) against UniProtKB/SwissProt (version 2014_11, 547,085 sequences). The research was carried out in all species. Spectra were searched with a mass tolerance of 15 ppm for MS and 0.05 Da for MS/MS data, allowing a maximum of one trypsin missed cleavage. Carbamidomethylation of cysteine residues and oxidation of methionine residues were specified as variable modifications. Protein identifications were validated with at least two peptides with Mascot ion score above 30.

3. Results

3.1. Nanoparticles behavior

The characterization of the primary nanoparticles has been published previously [28]. However, as we used DMEM in this work instead of RMPI in the previous one, we checked the hydrodynamic size and thus the aggregation state of the nanoparticles in serum-containing DMEM. The particles formed aggregates of 218±90 nm upon dilution in the medium, and the size of these aggregates decreased to 140±16 nm after 24 hours at 37°C in the serum-containing culture medium. This decrease in size has been previously observed in the same complete culture medium [52] and is consistent with the well-known dissolution of zinc oxide nanoparticles in culture media [52].

3.2. Proteomic results

The results of the proteomic analysis are shown on Figure 1 and Table 1. Out of the ca. 2550 spots reproducibly detected on the gels, 98 protein species were found modified in a statistically significant manner in at least one condition compared to the control. The t-test distributions of the various comparisons and a Venn diagram showing the overlap of changes between the different conditions (zinc oxide nanoparticles, zinc ion or zirconium oxide nanoparticles) are shown in supplementary figure 1. Only a few proteins species were quantitatively modulated by zirconium oxide, while many more were modulated by zinc oxide and zinc ion. Quite interestingly, 10 proteins species were modulated by all three treatments, 17 by both zinc oxide and zinc ion, 31 by zinc oxide only and 26 by zinc ion only. This result

goes against the dogma that zinc oxide toxicity is purely due to extracellular dissolution of zinc oxide [53] and support previous work showing differential effects of zinc oxide and zinc ions [54, 55].
In several cases (e.g. cytochrome bc1, ERP29, RhoGDI-2) one protein species was found statistically altered, generally the most acidic spot, while the more abundant, basic spot was found unmodified or weakly and insignificantly modified in abundance. In only a few cases (ETHE1, ETFA, hnRNP-K), several spots were found significantly changed in their abundance.

The modulated protein species could be sorted in several functional classes, which led us to investigate whether the biological/biochemical functions corresponding to these classes were also altered upon treatment with the nanoparticles.

3.3. Validation studies

3.3.1. Cytoskeleton and trafficking

Interesting changes were seen on some proteins involved in the actin cytoskeleton (dynactin, septin, Rho GDI, myosin) and in vesicular trafficking in the lysosomal pathway (e.g. NSF attachment factor, dynein). This led us to investigate both the actin cytoskeleton *per se* and the phagocytic activity of the cells. The results, displayed on Figures 2 and 3a, show the alteration brought by the metal oxide nanoparticles and/or by zinc ion.

Examination of the actin cytoskeleton by confocal microscopy (Figure 2) showed major alterations of this cellular component. First, the presence of nanoparticles in the medium induced the formation of numerous intracellular vesicles (arrows), which can be associated with the phagocytosis of the nanoparticles. The phenomenon was also observed with zinc ion, and can be related to the well-known formation of so-called zincosomes [56, 57]. This vesicle formation took place at the expense of the actin cortical layer, which is thinner in the nanoparticles-treated or zinc ion-treated cells compared to the control ones. The surface ruffles were also decreased in the treated cells compared to control cells. However, the cells treated with zinc, either zinc oxide nanoparticles or zinc ion, clearly showed a different, much rounder overall shape, thereby showing a major alteration of the actin cytoskeleton.
In line with these findings, the phagocytic activity (Figure 3a), a major natural function of macrophages, was not altered by zirconium oxide but strongly reduced by zinc treatment (ion or nanoparticle).

3.3.2. Mitochondria

One of the most prominent classes of modulated proteins consisted in mitochondrial proteins. The decrease of proteins of the mitochondrial protein production apparatus (e.g. ribosomal proteins) led us to hypothesize that the production of the mitochondrial respiratory complexes would also be decreased in turn, resulting in a change in the mitochondrial transmembrane potential. The results, displayed in Figure 3b, show that it is indeed the case, with a major effect of zinc oxide nanoparticles and almost no effect of zirconium oxide or of zinc ion.

3.3.3. The methylglyoxal pathway

Interestingly, three proteins involved in the detoxification of methyglyoxal (two aldose reductases and hydroxyacylglutathione hydrolase) were induced by zinc oxide nanoparticles, together with two proteins involved in the degradation of altered deoxyribonucleotides arising from DNA damage (deoxyribonucleotidase and deoxyribonucleotide N-hydrolase). As methylglyoxal production is known to increase when the carbohydrate metabolism is altered, we first investigated the inhibition of GAPDH by zinc. Zinc is known to inhibit purified GAPDH [58], and we first checked that the same effect occurs in complete cytosolic extracts, i.e. with the zinc buffering effects of the other cellular proteins. The results, displayed in Table 2, show that GAPDH in total extracts is inhibited at rather high zinc concentrations, in the range of the concentrations that we used in the present study. This led open the possibility that treatment with zinc oxide led to increased methylglyoxal production. If this hypothesis is true, zinc and methylglyoxal should show a synergistic toxicity, which we investigated. The results, displayed on Figure 4A, show that it is indeed the case, even if the effect seems moderate.

As methylglyoxal is known to bind to proteins and to the guanine nucleotide [59], the latter having putative long term consequences on DNA stability, we then investigated whether treatment of the cells with zinc oxide increased the level of methylglyoxal-modified nucleotides in DNA. The results, displayed on Figure 4B, show that zinc oxide doubles the amount of modified bases compared to the control, while zirconium oxide was without effect and methylglyoxal itself quadrupled the amount of these bases at the highest non toxic concentration. Interestingly, the effect of zinc ion on base modification was higher than the one of zinc oxide nanoparticles at equivalent zinc concentration.

4. Discussion

Zinc oxide is known for a long time for being mildly toxic, and has long be recognized as one of the causative agent for the professional disease called metal fume fever [4]. The threshold for the onset of the disease lies around 50-100 mg of zinc oxide per cubic meter of air. Using the classical respiration parameters (10 cubic meters of air inhaled per 8 hours day, alveolar penetration rate of 20-50% for nanoparticles) and the number of macrophages in the lungs, this translates into our exposure system to a 5-10ppm concentration range in the medium, and we took the 8µg/ml threshold as this corresponds to the LD20 concentration, i.e. a concentration where cell lethality begins to appear while the number of dead cells will not hamper the subsequent proteomic analysis.
Another toxic mechanism in lungs lies in the lung overload phenomenon (recently reviewed in [60]), occurring when a sufficient amount of inert, particulate material has been ingested by the alveolar macrophages. Transposed to in vitro systems [61], this impairment phenomenon begins to appear at 0.4 µg/mm2, while 0.2 µg/mm2 shows no effect. As the 8ppm dose that we used corresponds to a 0.22 µg/mm2 dose, this phenomenon can be excluded. The fact that the 10µg/ml dose of zirconium oxide did not produce any functional or toxic effect of macrophages also excludes this generic toxic mechanism, so that the effects observed in the case of zinc oxide can be attributed to the intrinsic properties of this nanoparticle.

The main interest to perform a comparative study is to sort out what is common in the

cellular responses and what is specific to each type of nanoparticles. In this frame, the changes common to both nanoparticles can be related to the modification of the cellular functioning induced by the phagocytosis event per se, as we already know that these precise nanoparticles are actively phagocytized by the cells [27], [28]. The quantitative changes in the protein species induced by phagocytosis represent only a very small proportion of the total changes observed. Apart from heme oxygenase, they include a few proteins linked to signalling, as a phosphatidyl inositol transfer protein, a phosphodiesterase, the dual specificity MAP kinase, the MOB kinase activator, and a few mitochondrial proteins, such as the stomatin like protein, one protein species for the electron transfer protein and one protein species for persulfide dioxygenase. Such a limited response is not surprising in a professional phagocyte, which is from the start well equipped to phagocytize particles.

There are few proteins species that are quantitatively modified by zirconium oxide only. They include one protein species of transaldolase and one protein species of cytochrome bc1 subunit 1, suggesting a mild alteration of metabolism. The changes in the amount of dual specificity map kinase 1 or PCNA are more difficult to interpret directly, but may be linked to a change in cell proliferation. The mild effects of zirconium oxide are likely linked to the fact that zirconium oxide does not have surface redox properties and does not dissolve to liberate toxic ions intracellularly, as zinc oxide does for example.

Zinc oxide induces indeed profound changes in the cellular responses, detected at the proteome level, but also as shown by the validation experiments.

Among such changes, the cytoskeleton/trafficking category is one of the most prominent, which is in line with the observed changes at the cytoskeletal and phagocytosis levels in the validation experiments. In this respect, the changes observed on RhoGDI2 are worth commenting in further details. RhoGDI2 is observed as two spots on the 2D gels (C3a and C3b) and only the acidic one is increased in response to zinc oxide. In the cell, RhoGDIs sequester the Rho and Rac GTPases in an inactive form [62], and this sequestration is released by the phosphorylation of RhoGDI [63, 64]. Thus, the increase of the acidic, phosphorylated protein species of RhoGDI2 likely translates into an increase in free, active Rac and Rho, showing the response of the cell to the effects of zinc on the actin cytoskeleton. This example illustrates the benefits of carrying out proteomics at the protein species level to explain the biological outcomes that are observed. Interestingly, this change in modified RhoGDI abundance was not observed with zinc ion, but other quantitative modulations affecting proteins involved in the actin cytoskeleton dynamics (e.g. capping proteins, cofilin or wdr1 protein) may lead to the similar outcome that we observed.

The protein regulating glutathione neosynthesis, GCLM, is also induced by zinc oxide and zinc ion, which is not surprising as glutathione is an important part in the cellular responses to thiophilic metals such as zinc [65], copper [66] and silver [67]. The heme oxygenase-ferritin pathway, the biliverdin reductase and the formylglutathione hydrolase also belong to these protective proteins increased in response to zinc oxide, but not necessarily in response to zinc ion.

Several perturbations can also be seen in various signalling pathways. One of the

striking examples is the decrease in inositol phosphate synthase, which is rate limiting for all inositol-containing molecules, so that the phosphoinositol-dependent signalling pathways may be impacted. In the same trend, RGS10, which is increased upon zinc oxide treatment of the cells, plays a role in macrophages functions and crosstalks with the inositol-dependent pathways [68].
Rather interestingly, we also observed an increase in the Myd88 protein, which is a key relay in TLR-dependent signalling. There is a close interplay between zinc and Myd88 [69, 70], so that the increase in the amount of Myd88 might correspond to an attempt of the cells to keep the pathway functional in the presence of high zinc levels.
Last but not least in the signalling area, a major increase in prostaglandin reductase was also observed. Via the PPAR-gamma pathway [71], this enzyme is linked to the energy metabolism.

Indeed, perturbations at the mitochondrial level are among the most striking alterations induced by zinc oxide. They are well documented on some mitochondrial dehydrogenases [72, 73] and further documented here at the level of the transmembrane potential, extending to macrophages the results already described on neurons [74] and on purified mitochondrial complexes [75].
Apart from its impact on mitochondria, zinc also impacts the central glycolytic metabolism at several levels [28, 29, 74, 76], with obvious consequences in terms of cellular energetics, thus explaining the protective effects of pyruvate and oxaloacetate [76, 77]. However, the further consequences of this impairment of the central glycolytic metabolism are generally not investigated.
Through our proteomic screen, we observed quantitative changes in some proteins (DNA repair proteins, glyoxalase 2, aldose reductase) that could be linked to this metabolic impairment via methylglyoxal. Methyglyoxal is produced from glyceraldehyde 3-phosphate by a natural phosphate elimination (Figure 5), mechanistically related to the well-known phosphoserine elimination, which is also divalent ion-catalyzed [78]. There is thus a competition between this reaction and the GAPDH-catalyzed glyceraldehyde 3-phosphate oxidation, so that the levels of methylglyoxal increase when the GAPDH activity decreases. In complex cellular extracts, GAPDH is inhibited at rather high zinc concentrations because of the general metal ion buffering capacity of proteins [79], but such high intracellular concentrations can be reached at still subtoxic zinc levels [28]. Moreover, we observed a decrease in the GAPDH activity in cells pretreated with zinc oxide, converging to a putative increase of the intracellular methylglyoxal levels. As the most deleterious effect of methylglyoxal resides in its ability to modify DNA bases, and especially guanine, we measured the amount of methylglyoxal-modified guanine in zinc oxide-treated cells and found a significant increase.

This raises the question of a possible carcinogenic effect of zinc, which has not been documented *in vivo* so far for mammals, and which is still controversial. A genotoxic effect of zinc has already been documented *in vitro* [7-11, 28, 80], but also *in vivo* [12, 13], although other studies do not reach the same conclusion (e.g. [14]), and our results may shed new light in this area. In fact, most of the genotoxicity studies primarily investigate the DNA strand break damages on the eukaryotic cells, either *ex vivo* or *in vitro*, using comet assays or more robust tests such as the micronuclei assay. The damages to bases are investigated by mutation reversal assays, generally carried out in bacteria. However, the results obtained on bacteria are valid on eukaryotic cells only if the metabolisms are comparable, and this explains while

the so-called metabolic activation of many organic chemicals must be carried out with liver fractions to generate the active metabolites that are not directly produced by the bacteria but are in mammalian systems. In the case of zinc, the metabolism is quite different between bacteria and eukaryotic cells. First, bacteria do not internalize nanoparticles, and they do not present the highly active intracellular zinc dissolution that takes place in lysosomes [57, 81]. Second, the general zinc ion metabolism is fairly different between bacteria and mammalian cells [56], especially phagocytes that store high amounts of zinc [82]. Thus, the glycation base damages that we demonstrate here as a result of zinc exposure are likely to be undetected in bacterial systems and will not induce massive strand breaks detectable by chromosomal aberrations or micronuclei tests.
Going into more details, the glycation base damages are known to be repaired by the nucleotide excision system [83], a system which end-products are dNMPs, including the ones bearing the damaged bases. The pool of dNMPS is sanitized in the cells by specialized enzymes, such as deoxyribonucleotidase or nucleotide N-hydrolase. We found an increase of deoxyribonucleotidase in response to both zinc oxide and zinc ion, while nucleotide N-hydrolase was increased only in response to zinc oxide. This may correlate, at least in part, with the lower amount of methylglyoxal-modified guanine found in the case of exposure to zinc oxide in comparison with exposure to the equivalent concentration of zinc ion. Furthermore, it must be kept in mind that methylglyoxal lesions are overcome by specialized polymerases [84]. However, these specialized polymerases introduce errors at other places in the DNA, so that zinc induces an overall burden of the DNA repair system at large. This may induce in turn an increased sensitivity to other DNA-damaging molecules, which then appear as the primary carcinogens.

This example of the methylglyoxal pathway, which is clearly linked to glycolytic metabolism, clearly poses the question of the influence of the cellular metabolism on the responses and sensitivities of cells to zinc. In this regard, it may be interesting to compare the results described here with those obtained on zinc ion and on the same zinc oxide nanomaterial [28], using a slightly different macrophage cell line (RAW264 instead of J774) but also a different medium (previously RPMI 1640 instead of high glucose DMEM). Interestingly, only a few proteins were found modulated in the same way between the two conditions (transaldolase, major vault protein, two proteasome regulators, GCLM, NSF attachment protein, sorting nexin 2 and RuvB-like 2 protein). At a higher level, the actin cytoskeleton at large and the proteasome system are altered in both cases, but this is detected through different proteins. However, more proteins involved in the central metabolism, mitochondria, and nucleotide metabolism are modulated in J774 cells grown in high glucose DMEM. We already mentioned that DMEM has a higher tryptophan content than RPMI, and this is known to have a pleiotropic effect on macrophages through the aryl hydrocarbon receptor [19, 22, 23]. As this receptor is stimulated by many ligands [17, 18], so that its activation may be relatively common in complex environments [21], the use of DMEM can be seen as an easy way to investigate this type of condition [20] without resorting to toxin agonists such as dioxins. However, high glucose DMEM is also twice richer in glucose than RPMI1640, and this may lead to a more active metabolism in cells grown in the richer medium. A more active metabolism could also explain the higher impact of the methylglyoxal pathway, and the higher impact on mitochondria observed with the richer medium.
These combined effects of zinc on the DNA and on glycolysis may indeed explain

why cancer cells, which are more dependent on glycolysis through the Warburg effect, are also in turn more sensitive to zinc than normal cells [85, 86]. This cross effect between glucose and zinc through the central metabolism may also be interesting to keep in mind when dealing with metabolic disorders.

Last but not least, it may be interesting to discuss the difference that are observed here between the responses to zinc oxide and those to zinc ion, while highly similar responses have been seen in other systems [53]. Taking into account the fact that previous work made on systems in which macrophages are important have also concluded to differences between the effects of zinc ion and zinc oxide, [54, 55], it is tempting to correlate these discrepancies with the phagocytic activity of the cells. In the case of T lymphocytes [53], which are very weakly endocytic, the zinc oxide is not internalized in the cells, and the only zinc which enters the cells is zinc ion coming from the outside and thus from the dissolution of the nanomaterial in the culture medium. In the case of macrophages, which are highly phagocytic, an important proportion of zinc is internalized directly in endosomes then in lysosomes, where it dissolves quickly [55, 81]. This may result in both a different kinetic of zinc increase in the cell, and a different subcellular localization of zinc. In fact, zinc coming directly from the outside of the cell in ionic form comes from the periphery to the center, while zinc coming from the intracellular dissolution comes from the center of the cell (the perinuclear region where the lysosomes are grouped) to more peripheral localizations. These different dynamics may explain why different impact are seen in phagocytic cells in response to zinc oxide and zinc ion.

5. Concluding remarks

Overall, this work underlines the interest but also the difficulties of protein species-based proteomics, as shown by the example of RhoGDI2. What we do observe on 2D gels is a quantitative modulation of a few spots, and after identification, we can get protein names on them. From the comparison of the theoretical pI and Mr of the proteins with the observed ones for the spots of interest we can often know if we are dealing with protein fragments or with intact proteins. However, even if we know that we are dealing with intact proteins, we seldom can know if we are dealing with a minor or a major form, with an inactive or an inactive form [67]. 2D blotting can provide useful information in terms of description of the landscape of protein species, but is not problem-free (antibodies cross-reactivities, maps realignments between 2D blots and stained patterns). Thus, an often-useful approach is to pick spots in the neigborhood of the quantitatively modified ones, as post-translationally modified spots are usually not far apart from each other. This is how we picked other forms of cytochrome bc1, ERP29 or RhoGDI2, just to name a few.

However, even a complete description of the protein species landscape usually does not give indication about the possible functional implications of the changes that we observed in our proteomic screens, and this is why we tested as much as possible the functional implications of the proteomic-derived findings in our case for understanding the toxicity of nanoparticles and in highlighting new mechanisms underlying this toxicity (e.g. the methylglyoxal pathway). The relative number of protein species modulated by two nanoparticles of different toxicities correlates with the toxicity, with much more proteins species changing in response to zinc oxide compared to zirconium dioxide. For zinc oxide, strong responses are shown for mitochondrial and cytoskeletal proteins, as well as in the methylglyoxal-detoxifying pathway, the latter suggesting a mechanism for zinc oxide genotoxicity.

ACKNOWLEDGEMENTS
The authors warmly thank Didier Grunwald and Isabelle Testard for their help in the confocal microscopy experiments. The financial support of the CEA toxicology program (Nanostress grants) and of ANSES (PNREST-2011-25 Innimunotox project) is also gratefully acknowledged. This work is a contribution to the Labex Serenade (n° ANR-11-LABX-0064) funded by the « Investissements d'Avenir» French Government program of the French National Research Agency (ANR) through the A*MIDEX project (n° ANR-11-IDEX-0001-02).

AUTHOR CONTRIBUTIONS
TR and VCF performed the proteomics experiments with nanoparticles. CAG performed the phagocytosis, mitochondria and the confocal microscopy experiments, and helped in drafting the manuscript. BD performed the nanomaterial characterization in culture medium, and part of the phagocytosis experiments. JLR and MC performed the dG-MG assay, helped in designing the whole study and in drafting the manuscript, and critically revised the manuscript. HD, JMS, SC and AVD performed and interpreted the mass spectrometry identification in the proteomics experiments, and helped in drafting the manuscript.
TR conceived and designed the whole study, took part in the proteomics experiments, performed the enzyme assays and drafted the manuscript. All authors read and approved the manuscript.

REFERENCES

[1] Zhang HY, Ji ZX, Xia T, Meng H, Low-Kam C, Liu R, et al. Use of Metal Oxide Nanoparticle Band Gap To Develop a Predictive Paradigm for Oxidative Stress and Acute Pulmonary Inflammation. Acs Nano. 2012;6:4349-68.
[2] Applerot G, Lellouche J, Perkas N, Nitzan Y, Gedanken A, Banin E. ZnO nanoparticle-coated surfaces inhibit bacterial biofilm formation and increase antibiotic susceptibility. Rsc Advances. 2012;2:2314-21.
[3] Osmond MJ, McCall MJ. Zinc oxide nanoparticles in modern sunscreens: An analysis of potential exposure and hazard. Nanotoxicology. 2010;4:15-41.
[4] Drinker P, Thomson RM, Finn JL. Metal Fume Fever: IV. Threshold Doses of Zinc Oxide, Preventive Measures, and the Chronic Effects of Repeated Exposures. Journal of Industrial Hygiene. 1927;9:331-45.
[5] Rohrs LC. Metal-fume fever from inhaling zinc oxide. AMA Arch Ind Health. 1957;16:42-7.
[6] Huang CC, Aronstam RS, Chen DR, Huang YW. Oxidative stress, calcium homeostasis, and altered gene expression in human lung epithelial cells exposed to ZnO nanoparticles. Toxicology in Vitro. 2010;24:45-55.
[7] Sharma V, Anderson D, Dhawan A. Zinc Oxide Nanoparticles Induce Oxidative Stress and Genotoxicity in Human Liver Cells (HepG2). Journal of Biomedical Nanotechnology. 2011;7:98-9.
[8] Hackenberg S, Scherzed A, Technau A, Kessler M, Froelich K, Ginzkey C, et al. Cytotoxic, genotoxic and pro-inflammatory effects of zinc oxide nanoparticles in human nasal mucosa cells in vitro. Toxicol In Vitro. 2011;25:657-63.
[9] Senapati VA, Kumar A, Gupta GS, Pandey AK, Dhawan A. ZnO nanoparticles induced inflammatory response and genotoxicity in human blood cells: A mechanistic approach. Food Chem Toxicol. 2015.

[10] Heim J, Felder E, Tahir MN, Kaltbeitzel A, Heinrich UR, Brochhausen C, et al. Genotoxic effects of zinc oxide nanoparticles. Nanoscale. 2015;7:8931-8.
[11] Zijno A, De Angelis I, De Berardis B, Andreoli C, Russo MT, Pietraforte D, et al. Different mechanisms are involved in oxidative DNA damage and genotoxicity induction by ZnO and TiO2 nanoparticles in human colon carcinoma cells. Toxicol In Vitro. 2015;29:1503-12.
[12] Ali D, Alarifi S, Kumar S, Ahamed M, Siddiqui MA. Oxidative stress and genotoxic effect of zinc oxide nanoparticles in freshwater snail Lymnaea luteola L. Aquat Toxicol. 2012;124-125:83-90.
[13] Carmona ER, Inostroza-Blancheteau C, Rubio L, Marcos R. Genotoxic and oxidative stress potential of nanosized and bulk zinc oxide particles in Drosophila melanogaster. Toxicol Ind Health. 2015.
[14] Kwon JY, Lee SY, Koedrith P, Lee JY, Kim KM, Oh JM, et al. Lack of genotoxic potential of ZnO nanoparticles in in vitro and in vivo tests. Mutat Res Genet Toxicol Environ Mutagen. 2014;761:1-9.
[15] Palomaki J, Karisola P, Pylkkanen L, Savolainen K, Alenius H. Engineered nanornaterials cause cytotoxicity and activation on mouse antigen presenting cells. Toxicology. 2010;267:125-31.
[16] Denison MS, Vella LM. The hepatic Ah receptor for 2,3,7,8-tetrachlorodibenzo-p-dioxin: species differences in subunit dissociation. Arch Biochem Biophys. 1990;277:382-8.
[17] Adachi J, Mori Y, Matsui S, Takigami H, Fujino J, Kitagawa H, et al. Indirubin and indigo are potent aryl hydrocarbon receptor ligands present in human urine. J Biol Chem. 2001;276:31475-8.
[18] Heath-Pagliuso S, Rogers WJ, Tullis K, Seidel SD, Cenijn PH, Brouwer A, et al. Activation of the Ah receptor by tryptophan and tryptophan metabolites. Biochemistry. 1998;37:11508-15.
[19] Opitz CA, Litzenburger UM, Sahm F, Ott M, Tritschler I, Trump S, et al. An endogenous tumour-promoting ligand of the human aryl hydrocarbon receptor. Nature. 2011;478:197-203.
[20] Veldhoen M, Hirota K, Christensen J, O'Garra A, Stockinger B. Natural agonists for aryl hydrocarbon receptor in culture medium are essential for optimal differentiation of Th17 T cells. J Exp Med. 2009;206:43-9.
[21] Esser C, Rannug A. The aryl hydrocarbon receptor in barrier organ physiology, immunology, and toxicology. Pharmacol Rev. 2015;67:259-79.
[22] Esser C, Rannug A, Stockinger B. The aryl hydrocarbon receptor in immunity. Trends Immunol. 2009;30:447-54.
[23] Cohly H, Stephens J, Markhov A, Angel M, Campbell W, Ndebele K, et al. Cell culture conditions affect LPS inducibility of the inflammatory mediators in J774A.1 murine macrophages. Immunol Invest. 2001;30:1-15.
[24] Rabilloud T, Lescuyer P. Proteomics in mechanistic toxicology: history, concepts, achievements, caveats, and potential. Proteomics. 2015;15:1051-74.
[25] Verano-Braga T, Miethling-Graff R, Wojdyla K, Rogowska-Wrzesinska A, Brewer JR, Erdmann H, et al. Insights into the cellular response triggered by silver nanoparticles using quantitative proteomics. ACS Nano. 2014;8:2161-75.
[26] Edelmann MJ, Shack LA, Naske CD, Walters KB, Nanduri B. SILAC-based quantitative proteomic analysis of human lung cell response to copper oxide nanoparticles. PLoS One. 2014;9:e114390.
[27] Triboulet S, Aude-Garcia C, Carriere M, Diemer H, Proamer F, Habert A, et al. Molecular responses of mouse macrophages to copper and copper oxide

nanoparticles inferred from proteomic analyses. Mol Cell Proteomics. 2013;12:3108-22.
[28] Triboulet S, Aude-Garcia C, Armand L, Gerdil A, Diemer H, Proamer F, et al. Analysis of cellular responses of macrophages to zinc ions and zinc oxide nanoparticles: a combined targeted and proteomic approach. Nanoscale. 2014;6:6102-14.
[29] Filippi C, Pryde A, Cowan P, Lee T, Hayes P, Donaldson K, et al. Toxicology of ZnO and TiO2 nanoparticles on hepatocytes: Impact on metabolism and bioenergetics. Nanotoxicology. 2015;9:126-34.
[30] Triboulet S, Aude-Garcia C, Armand L, Collin-Faure V, Chevallet M, Diemer H, et al. Comparative proteomic analysis of the molecular responses of mouse macrophages to titanium dioxide and copper oxide nanoparticles unravels some toxic mechanisms for copper oxide nanoparticles in macrophages. PLoS One. 2015;10:e0124496.
[31] Abel G, Szollosi J, Fachet J. Phagocytosis of fluorescent latex microbeads by peritoneal macrophages in different strains of mice: a flow cytometric study. Eur J Immunogenet. 1991;18:239-45.
[32] Reers M, Smith TW, Chen LB. J-aggregate formation of a carbocyanine as a quantitative fluorescent indicator of membrane potential. Biochemistry. 1991;30:4480-6.
[33] Donaghy L, Kraffe E, Le Goic N, Lambert C, Volety AK, Soudant P. Reactive oxygen species in unstimulated hemocytes of the pacific oyster Crassostrea gigas: a mitochondrial involvement. PLoS One. 2012;7:e46594.
[34] Bradford MM. A rapid and sensitive method for the quantitation of microgram quantities of protein utilizing the principle of protein-dye binding. Anal Biochem. 1976;72:248-54.
[35] Mayer KM, Arnold FH. A colorimetric assay to quantify dehydrogenase activity in crude cell lysates. J Biomol Screen. 2002;7:135-40.
[36] Ravanat JL. Chromatographic methods for the analysis of oxidatively damaged DNA. Free Radic Res. 2012;46:479-91.
[37] Ravanat JL, Douki T, Duez P, Gremaud E, Herbert K, Hofer T, et al. Cellular background level of 8-oxo-7,8-dihydro-2'-deoxyguanosine: an isotope based method to evaluate artefactual oxidation of DNA during its extraction and subsequent work-up. Carcinogenesis. 2002;23:1911-8.
[38] Yuan B, Cao H, Jiang Y, Hong H, Wang Y. Efficient and accurate bypass of N2-(1-carboxyethyl)-2'-deoxyguanosine by DinB DNA polymerase in vitro and in vivo. Proc Natl Acad Sci U S A. 2008;105:8679-84.
[39] Gianazza E, Celentano F, Magenes S, Ettori C, Righetti PG. Formulations for immobilized pH gradients including pH extremes. Electrophoresis. 1989;10:806-8.
[40] Rabilloud T, Valette C, Lawrence JJ. Sample application by in-gel rehydration improves the resolution of two-dimensional electrophoresis with immobilized pH gradients in the first dimension. Electrophoresis. 1994;15:1552-8.
[41] Rabilloud T, Adessi C, Giraudel A, Lunardi J. Improvement of the solubilization of proteins in two-dimensional electrophoresis with immobilized pH gradients. Electrophoresis. 1997;18:307-16.
[42] Luche S, Diemer H, Tastet C, Chevallet M, Van Dorsselaer A, Leize-Wagner E, et al. About thiol derivatization and resolution of basic proteins in two-dimensional electrophoresis. Proteomics. 2004;4:551-61.
[43] Gorg A, Postel W, Weser J, Gunther S, Strahler JR, Hanash SM, et al. Elimination of Point Streaking on Silver Stained Two-Dimensional Gels by Addition of

Iodoacetamide to the Equilibration Buffer. Electrophoresis. 1987;8:122-4.
[44] Olsson I, Larsson K, Palmgren R, Bjellqvist B. Organic disulfides as a means to generate streak-free two-dimensional maps with narrow range basic immobilized pH gradient strips as first dimension. Proteomics. 2002;2:1630-2.
[45] Tastet C, Lescuyer P, Diemer H, Luche S, van Dorsselaer A, Rabilloud T. A versatile electrophoresis system for the analysis of high- and low-molecular-weight proteins. Electrophoresis. 2003;24:1787-94.
[46] Sinha P, Poland J, Schnolzer M, Rabilloud T. A new silver staining apparatus and procedure for matrix-assisted laser desorption/ionization-time of flight analysis of proteins after two-dimensional electrophoresis. Proteomics. 2001;1:835-40.
[47] Herrmann AG, Searcy JL, Le Bihan T, McCulloch J, Deighton RF. Total variance should drive data handling strategies in third generation proteomic studies. Proteomics. 2013;13:3251-5.
[48] Storey JD, Tibshirani R. Statistical significance for genomewide studies. Proc Natl Acad Sci U S A. 2003;100:9440-5.
[49] Diz AP, Carvajal-Rodriguez A, Skibinski DO. Multiple hypothesis testing in proteomics: a strategy for experimental work. Mol Cell Proteomics. 2011;10:M110 004374.
[50] Gharahdaghi F, Weinberg CR, Meagher DA, Imai BS, Mische SM. Mass spectrometric identification of proteins from silver-stained polyacrylamide gel: A method for the removal of silver ions to enhance sensitivity. Electrophoresis. 1999;20:601-5.
[51] Richert S, Luche S, Chevallet M, Van Dorsselaer A, Leize-Wagner E, Rabilloud T. About the mechanism of interference of silver staining with peptide mass spectrometry. Proteomics. 2004;4:909-16.
[52] Meissner T, Oelschlagel K, Potthoff A. Implications of the stability behavior of zinc oxide nanoparticles for toxicological studies. International Nano Letters C7 - 116. 2014;4:1-13.
[53] Tuomela S, Autio R, Buerki-Thurnherr T, Arslan O, Kunzmann A, Andersson-Willman B, et al. Gene Expression Profiling of Immune-Competent Human Cells Exposed to Engineered Zinc Oxide or Titanium Dioxide Nanoparticles. Plos One. 2013;8.
[54] Cho WS, Duffin R, Poland CA, Duschl A, Oostingh GJ, MacNee W, et al. Differential pro-inflammatory effects of metal oxide nanoparticles and their soluble ions in vitro and in vivo; zinc and copper nanoparticles, but not their ions, recruit eosinophils to the lungs. Nanotoxicology. 2012;6:22-35.
[55] Cho WS, Duffin R, Howie SEM, Scotton CJ, Wallace WAH, MacNee W, et al. Progressive severe lung injury by zinc oxide nanoparticles; the role of Zn2+ dissolution inside lysosomes. Particle and Fibre Toxicology. 2011;8.
[56] Eide DJ. Zinc transporters and the cellular trafficking of zinc. Biochim Biophys Acta. 2006;1763:711-22.
[57] Wellenreuther G, Cianci M, Tucoulou R, Meyer-Klaucke W, Haase H. The ligand environment of zinc stored in vesicles. Biochem Biophys Res Commun. 2009;380:198-203.
[58] Krotkiewska B, Banas T. Interaction of Zn2+ and Cu2+ ions with glyceraldehyde-3-phosphate dehydrogenase from bovine heart and rabbit muscle. Int J Biochem. 1992;24:1501-5.
[59] Chaplen FW. Incidence and potential implications of the toxic metabolite methylglyoxal in cell culture: A review. Cytotechnology. 1998;26:173-83.
[60] Borm P, Cassee FR, Oberdorster G. Lung particle overload: old school -new

insights? Part Fibre Toxicol. 2015;12:10.
[61] Renwick LC, Donaldson K, Clouter A. Impairment of alveolar macrophage phagocytosis by ultrafine particles. Toxicol Appl Pharmacol. 2001;172:119-27.
[62] Garcia-Mata R, Boulter E, Burridge K. The 'invisible hand': regulation of RHO GTPases by RHOGDIs. Nat Rev Mol Cell Biol. 2011;12:493-504.
[63] DerMardirossian C, Schnelzer A, Bokoch GM. Phosphorylation of RhoGDI by Pak1 mediates dissociation of Rac GTPase. Mol Cell. 2004;15:117-27.
[64] DerMardirossian C, Rocklin G, Seo JY, Bokoch GM. Phosphorylation of RhoGDI by Src regulates Rho GTPase binding and cytosol-membrane cycling. Mol Biol Cell. 2006;17:4760-8.
[65] Seagrave J, Tobey RA, Hildebrand CE. Zinc effects on glutathione metabolism relationship to zinc-induced protection from alkylating agents. Biochem Pharmacol. 1983;32:3017-21.
[66] Freedman JH, Ciriolo MR, Peisach J. The role of glutathione in copper metabolism and toxicity. J Biol Chem. 1989;264:5598-605.
[67] Veronesi G, Aude-Garcia C, Kieffer I, Gallon T, Delangle P, Herlin-Boime N, et al. Exposure-dependent Ag(+) release from silver nanoparticles and its complexation in AgS2 sites in primary murine macrophages. Nanoscale. 2015;7:7323-30.
[68] Yang S, Li YP. RGS10-null mutation impairs osteoclast differentiation resulting from the loss of [Ca2+]i oscillation regulation. Genes Dev. 2007;21:1803-16.
[69] Brieger A, Rink L, Haase H. Differential regulation of TLR-dependent MyD88 and TRIF signaling pathways by free zinc ions. J Immunol. 2013;191:1808-17.
[70] Chang H, Ho CC, Yang CS, Chang WH, Tsai MH, Tsai HT, et al. Involvement of MyD88 in zinc oxide nanoparticle-induced lung inflammation. Exp Toxicol Pathol. 2013;65:887-96.
[71] Chou WL, Chuang LM, Chou CC, Wang AH, Lawson JA, FitzGerald GA, et al. Identification of a novel prostaglandin reductase reveals the involvement of prostaglandin E2 catabolism in regulation of peroxisome proliferator-activated receptor gamma activation. J Biol Chem. 2007;282:18162-72.
[72] Brown AM, Kristal BS, Effron MS, Shestopalov AI, Ullucci PA, Sheu KF, et al. Zn2+ inhibits alpha-ketoglutarate-stimulated mitochondrial respiration and the isolated alpha-ketoglutarate dehydrogenase complex. J Biol Chem. 2000;275:13441-7.
[73] Gazaryan IG, Krasnikov BF, Ashby GA, Thorneley RN, Kristal BS, Brown AM. Zinc is a potent inhibitor of thiol oxidoreductase activity and stimulates reactive oxygen species production by lipoamide dehydrogenase. J Biol Chem. 2002;277:10064-72.
[74] Dineley KE, Votyakova TV, Reynolds IJ. Zinc inhibition of cellular energy production: implications for mitochondria and neurodegeneration. J Neurochem. 2003;85:563-70.
[75] Martino PL, Capitanio G, Capitanio N, Papa S. Inhibition of proton pumping in membrane reconstituted bovine heart cytochrome c oxidase by zinc binding at the inner matrix side. Biochim Biophys Acta. 2011;1807:1075-82.
[76] Sheline CT, Behrens MM, Choi DW. Zinc-induced cortical neuronal death: contribution of energy failure attributable to loss of NAD(+) and inhibition of glycolysis. J Neurosci. 2000;20:3139-46.
[77] Berry EV, Toms NJ. Pyruvate and oxaloacetate limit zinc-induced oxidative HT-22 neuronal cell injury. Neurotoxicology. 2006;27:1043-51.
[78] Byford MF. Rapid and selective modification of phosphoserine residues catalysed by Ba2+ ions for their detection during peptide microsequencing. Biochem

J. 1991;280 (Pt 1):261-5.
[79] Haase H, Hebel S, Engelhardt G, Rink L. The biochemical effects of extracellular Zn(2+) and other metal ions are severely affected by their speciation in cell culture media. Metallomics. 2015;7:102-11.
[80] Sharma V, Shukla RK, Saxena N, Parmar D, Das M, Dhawan A. DNA damaging potential of zinc oxide nanoparticles in human epidermal cells. Toxicol Lett. 2009;185:211-8.
[81] James SA, Feltis BN, de Jonge MD, Sridhar M, Kimpton JA, Altissimo M, et al. Quantification of ZnO nanoparticle uptake, distribution, and dissolution within individual human macrophages. ACS Nano. 2013;7:10621-35.
[82] Subramanian Vignesh K, Landero Figueroa JA, Porollo A, Caruso JA, Deepe GS, Jr. Zinc sequestration: arming phagocyte defense against fungal attack. PLoS Pathog. 2013;9:e1003815.
[83] Tamae D, Lim P, Wuenschell GE, Termini J. Mutagenesis and repair induced by the DNA advanced glycation end product N2-1-(carboxyethyl)-2'-deoxyguanosine in human cells. Biochemistry. 2011;50:2321-9.
[84] Yuan B, You C, Andersen N, Jiang Y, Moriya M, O'Connor TR, et al. The roles of DNA polymerases kappa and iota in the error-free bypass of N2-carboxyalkyl-2'-deoxyguanosine lesions in mammalian cells. J Biol Chem. 2011;286:17503-11.
[85] Sliwinski T, Czechowska A, Kolodziejczak M, Jajte J, Wisniewska-Jarosinska M, Blasiak J. Zinc salts differentially modulate DNA damage in normal and cancer cells. Cell Biol Int. 2009;33:542-7.
[86] Costello LC, Franklin RB. Cytotoxic/tumor suppressor role of zinc for the treatment of cancer: an enigma and an opportunity. Expert Rev Anticancer Ther. 2012;12:121-8.

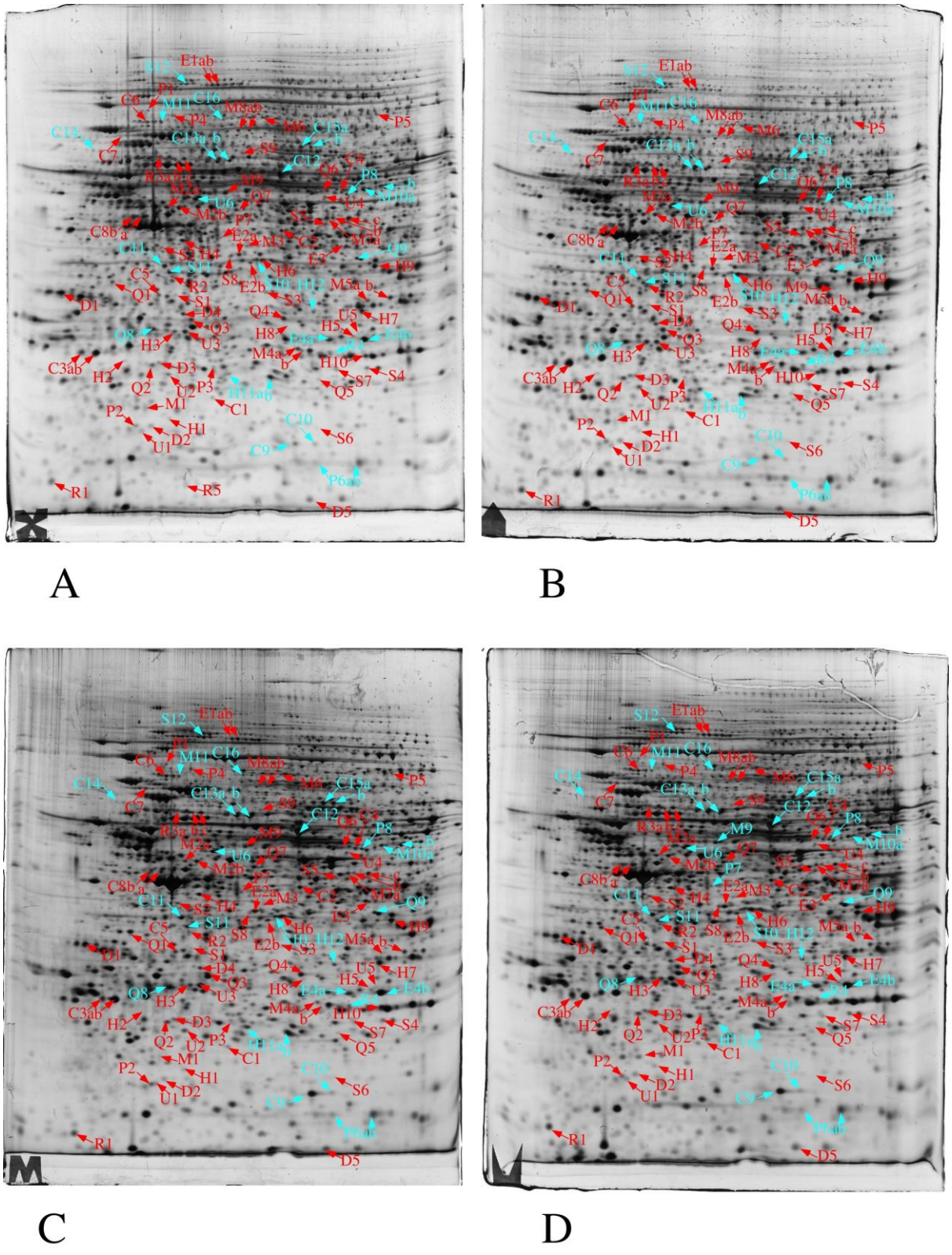


Figure 1: Proteomic analysis of total cell extracts by 2D electrophoresis

Total cell extracts of J774A1 cells were separated by two-dimensional gel electrophoresis. The first dimensions covered a 4-8 pH range and the second dimension a 15-200 kDa range. Total cellular proteins (150 µg) were loaded on the first dimension gel.

A: gel obtained from control cells
B: gel obtained from cells treated with cationic zinc oxide (8 µg/ml, 24 hours)
C: gel obtained from cells treated with zirconium oxide (10 µg/ml, 24 hours)
D: gel obtained from cells treated with zinc acetate (100µM, 24 hours)

The red arrows point to spots that show reproducible and statistically significant changes between the control and nanoparticles-treated cells and to the control neighbor spots in some cases. The blue arrows point to spots that show reproducible and statistically significant changes between the control and zinc ion-treated cells and to the control neighbor spots in some cases. Spot numbering according to Table 1.

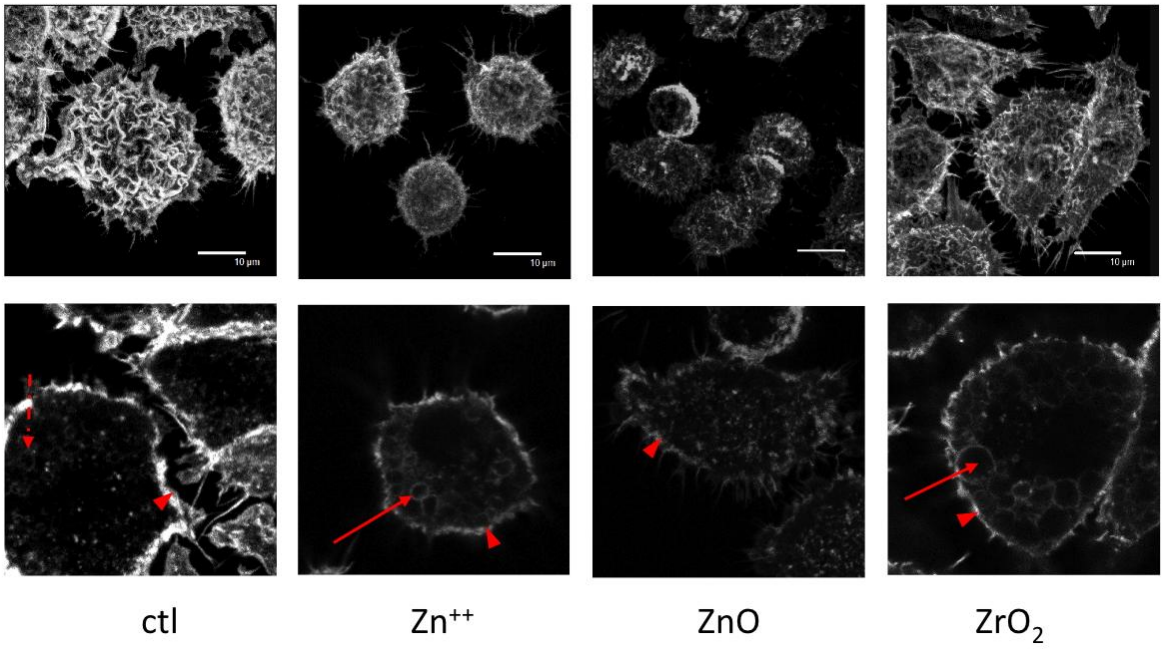


Figure 2: confocal imaging of the F-actin cytoskeleton
In the top row, 3D reconstructions of the F-actin cytoskeleton are shown, allowing visualization of the surface ruffles of the cells.
The bottom row shows one confocal plane inside the cells. The arrows point to the internal vesicles in the cells, while the arrowheads point to the cortical actin layer.
Ctrl: control cells
ZnO: cells treated with 8µg/ml zinc oxide
Zn ion: cells treated with 100µM zinc acetate
ZrO2: cells treated with 10µg/ml zirconium oxide

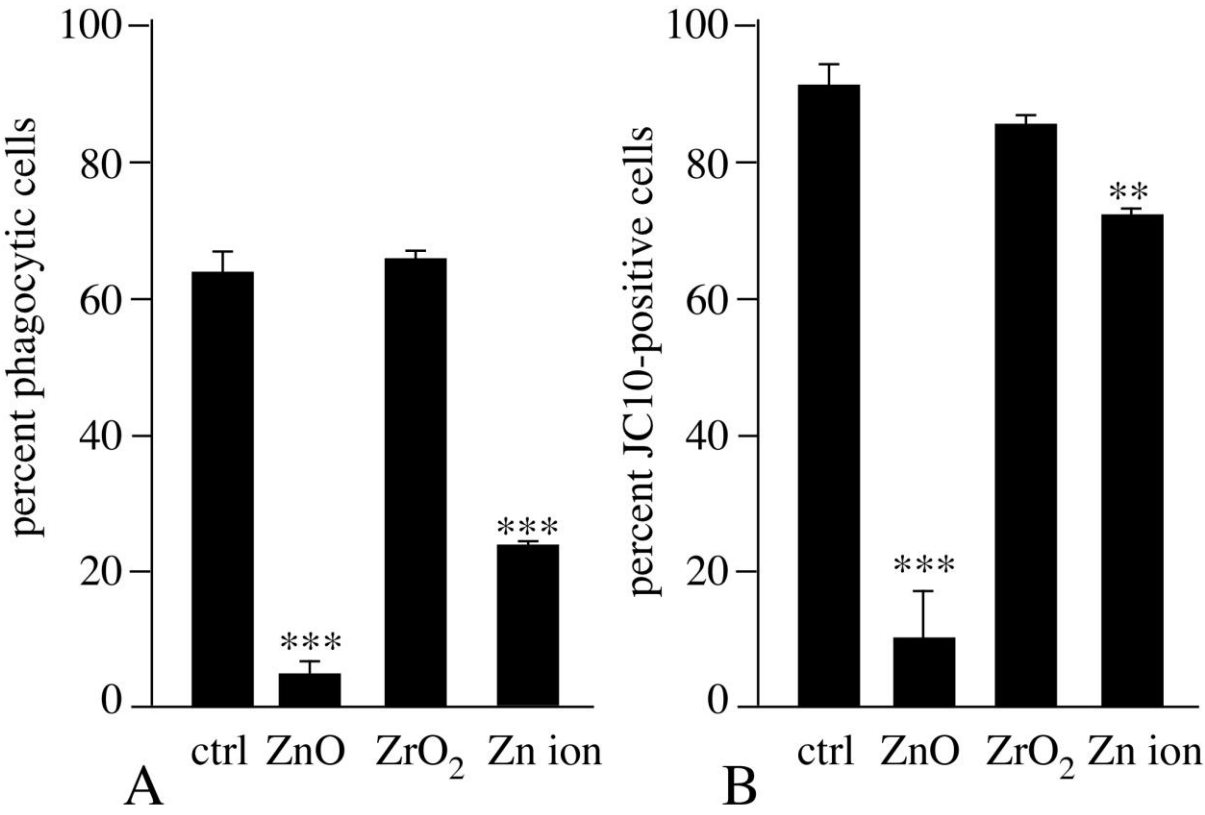


Figure 3: Phagocytic activity and mitochondrial transmembrane potential of J774 cells upon treatment with nanoparticles

3A: assay of the phagocytic activity index (3 independent experiments).

3B; percentage of JC-10 positive cells in the cultures, i.e. cells with a normal mitochondrial potential (3 independent experiments). Fluorescence measurements were carried out on a FACScalibur cell sorter.

Statistical confidence (Student T-test) is indicated as follows: ** p≤0.01; *** p≤ 0.001

Ctrl: control cells
ZnO: cells treated with 8µg/ml zinc oxide
ZrO2: cells treated with 10µg/ml zirconium oxide
Zn ion: cells treated with 100µM zinc acetate

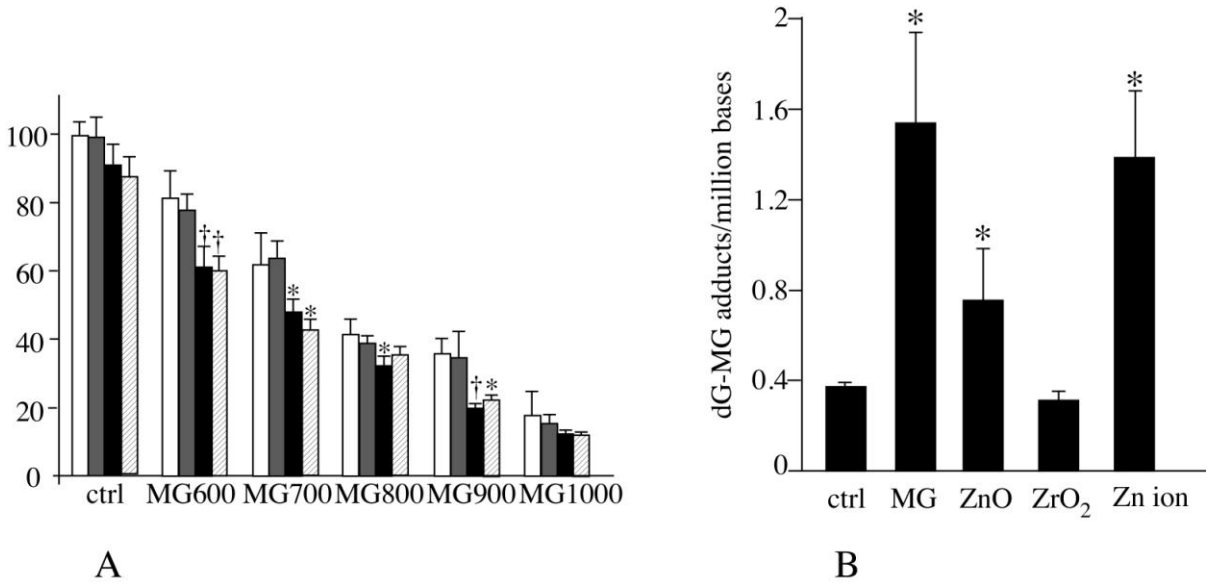


Figure 4: Zinc oxide and methylglyoxal

In panel A, J774 cells were treated for 24 hours as indicated (6 hours pre-incubation with nanoparticles + 18 hours in presence of variable concentrations of methylglyoxal indicated in µM). The viability was measured by the trypan blue exclusion assay
White bars : control cells (no nanoparticles added)
Grey bars : cells treated with 10µg/ml zirconium oxide
Black bars : cells treated with 8µg/ml zinc oxide
Hatched bars: cells treated with 100µM zinc acetate

In panel B, the amount of methylglyoxal-modified guanine was measured after treatment of the cells for 24 hours by the indicated compounds

Ctrl: control cells
MG: cells treated with 600µM methylgloxal
ZrO2: cells treated with 10µg/ml zirconium oxide
ZnO: cells treated with 8µg/ml zinc oxide
Zn ion: cells treated with 100µM zinc acetate

For both panels, measurements were carried out on biological triplicates . Statistical confidence (Student T-test vs. control) is indicated as follows: *: $p \leq 0.05$; † $p \leq 0.01$

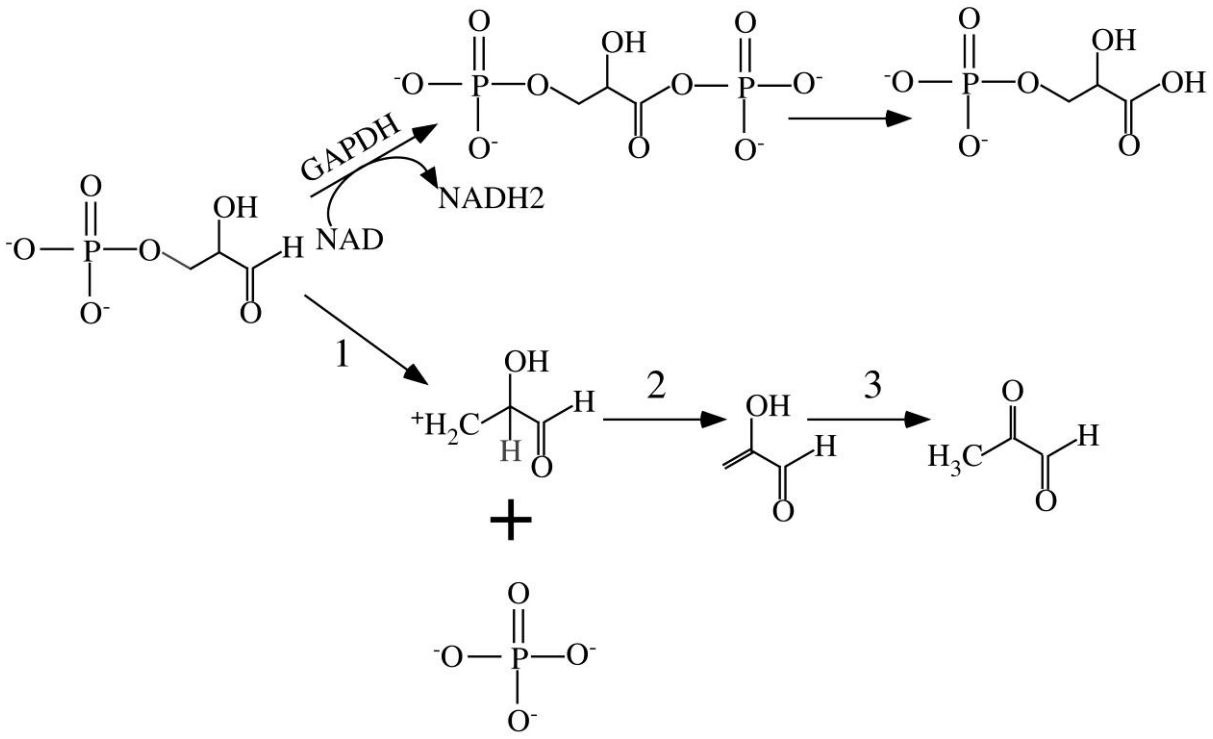


Figure 5: Generation of methylglyoxal from glyceraldehyde phosphate
In the physiological, GAPDH-catalyzed reaction (top pathway) the oxidation catalyzed by the GAPDH destroys the terminal aldehyde function of the glyceraldehyde, so that even chemical hydrolysis of the 1,3 diphosphoglycerate will yield a non toxic carboxylic acid.
In the bottom pathway, the labile bonds or atoms are shown in blue. The phosphoester is prone to asymmetric bond cleavage, with generation of an unstable carbocation (1). The hydrogen in the alpha position of the terminal carbonyl function is highly labile, which drives the overall reaction to a beta elimination of phosphoric acid (2). The beta elimination product being an enol, it isomerizes to the dicarbonyl compound (3) yielding to methylglyoxal.
As in the case of phosphoserine, where the same beta elimination reaction can take place, divalent cations, which bind to the phosphate, catalyze the elimination reaction. Thus, high levels of intracellular zinc have a dual effect in inhibiting the GAPDH-catalyzed pathway and driving the beta elimination pathway at the same time.